

# HST/WFPC2 proper motions in two bulge fields: kinematics and stellar population of the Galactic bulge<sup>1</sup>

Konrad Kuijken

*Kapteyn Institute, PO Box 800, 9700 AV Groningen, The Netherlands*<sup>2</sup>

kuijken@astro.rug.nl

and

R. Michael Rich

*Division of Astronomy, Department of Physics and Astronomy, UCLA, LA CA 90095-1562*

rmr@astro.ucla.edu

## ABSTRACT

We report proper motion dispersions for stars in the direction of two fields of the Galactic bulge, using HST/WFPC2 images taken six years apart. Our two fields are Baade's Window  $(l, b) = (1.13^\circ, -3.77^\circ)$  and Sgr I  $(l, b) = (1.25^\circ, -2.65^\circ)$ . Our proper motion dispersions are in good agreement with prior ground- and space-based proper motion studies in bulge fields, but in contrast to some prior studies, we do not exclude any subset of stars from our studies. In Baade's Window, we find the  $l$  and  $b$  proper motion dispersions are 2.9 and 2.5 mas/yr, while in Sgr I, they are 3.3 and 2.7 mas/yr, respectively. For the first time, we can clearly separate the foreground disk stars out from the bulge because of their large mean apparent proper motion. The population with non-disk kinematics (which we conclude to be the bulge) has an old main sequence turnoff point, similar to those found in old, metal rich bulge globular clusters while those stars selected to have disk kinematics lie on a fully populated main sequence. Separating main sequence stars by luminosity, we find strong evidence that the bulge population is rotating, largely explaining observations of proper motion anisotropy in bulge fields. Because we have isolated such a pure sample of stars in the bulge, we have one of the clearest demonstrations that the old stellar population of the inner bulge/bar is in fact rotating.

---

<sup>1</sup>Based on observations made with the NASA/ESA Hubble Space Telescope, obtained at the Space Telescope Science Institute, which is operated by the Association of Universities for Research in Astronomy, Inc., under NASA contract NAS 5-2655. These observations are associated with proposal GO-8250.

<sup>2</sup>Visiting scientist, Dept. of Theoretical Physics, Univ. of the Basque Country

*Subject headings:* Galaxy: bulge, kinematics and dynamics, stellar content; methods: data analysis

## 1. Introduction

The bulge of our Galaxy is interesting for a number of reasons. It is the nearest galactic bulge to the sun, and represents a unique place to study the stellar populations and stellar dynamics of such objects in detail. Such analysis can provide important information for our understanding of how bulges formed their stellar populations, what gravitational potential they sit in, and how they came to have the structure they do. In the case of our Galactic bulge, stellar motions are of great interest both in testing the hypothesis that our bulge is in fact a bar (e.g. Zhao, Rich, & Spergel 1996) and in the modeling of microlenses, the overwhelming majority of which are seen in the direction of the bulge (Alcock et al. 2000).

There are several complications in trying to build an understanding of our bulge. Close to the galactic plane, extinction by foreground dust is large and uneven (even on very small scales) and effectively limits optical work to a few “windows” of low and relatively uniform extinction. More troubling is the difficulty that the stellar population seen in these directions samples everything along the line of sight. Simple exponential models for the disk, for example, predict that in Baade’s Window at least half of the stars visible are actually disk stars, and not bulge stars. Employing photometry alone, it is not possible to effectively sort the populations; bulge and disk populations overlap in color, especially near the turnoff (Holtzman et al. 1998) greatly complicating the use of HST-derived CMDs for age determination. Blue stragglers extending brighter than the turnoff in an old population overlap with the main sequence locus of a young population.

Among the first stellar populations imaged in 1994 with the repaired WFPC2 on board HST were fields near two of the low extinction regions originally identified by Walter Baade: what is now known as Baade’s Window  $(l, b) = (1.13^\circ, -3.77^\circ)$ , and Sgr I  $(l, b) = (1.25^\circ, -2.65^\circ)$ . A discussion of the photometry and luminosity function of the Baade’s Window field is given in Holtzman et al. (1998).

We noticed that the fields were ripe for a revisit with the aim of measuring proper motions and we proposed successfully (GO-8250). Although HST has been used to measure proper motions of field stars in the rough vicinity of the Galactic Center, these two fields are of special interest because they lie well within the *COBE* bulge (Dwek et al. 1995) and, in the case of Baade’s Window, abundances are measured (McWilliam & Rich 1994) and many other studies have been done. Combining proper motions with precision photometry might make it possible to separate the observed populations based on their kinematics. The only previous study of bulge proper motions in Baade’s Window was based on photographic plates (Spaenhauer, Jones, & Whitford 1992) and

reported motions only of stars thought to be candidate red giants in the bulge, by Arp (1965). By systematically excluding the bluer disk stars, and by only measuring a few hundred of the brightest giants, this study, while pioneering, leaves much of the problem ripe for inquiry. Hence our decision to obtain second epoch images of both bulge fields, using WFPC2 on board HST.

## 2. Observations and proper motion measurements

In August of 2000 we obtained HST/WFPC2 observations of two bulge fields for which archival images suitable as first-epoch observations existed. The coordinates and observations are listed in Table 1.

The archival data, though they consist of multiple exposures, are not dithered. This compromises our ability to centroid stars accurately, as the images on the wide-field camera CCDs are very much undersampled. We therefore chose to observe the second epoch data (henceforth referred to as Y2K data) in the F814W filter, which gives the widest, and hence least undersampled, point-spread function (PSF). We also decided to dither the Y2K exposures in a regular 2x2 pattern of offsets (with a step of 0.55 arcsec, or 5.5 pixels on the WF CCDs), ensuring that the uncertainties in the proper motions would not be dominated by the newer epoch.

It is easy to show that the  $1\text{-}\sigma$  uncertainty in the centroid of a stellar image of full-width at half maximum FWHM that is detected at significance (S/N) is given by

$$0.7 \times \text{FWHM}/(\text{S/N})$$

where the numerical coefficient has a constant value for Moffat-profile PSF's with asymptotic power-law slopes ranging from 2 to infinity, the latter corresponding to a gaussian PSF (see Appendix). With HST, therefore (FWHM  $\simeq$  0.12arcsec in F814W), a star detected at  $25\text{-}\sigma$  could be centered to about 3.4mas (1/30th of a pixel). Over a 7-year baseline, proper motions can be measured for such stars to an accuracy of 0.7mas/yr. At the distance to the bulge of about 8kpc this corresponds to about 25km/s.

Table 1: HST/WFPC2 data used in this paper

Field	Epoch	Exp (s)	Remarks	$\alpha, \delta$ (2000)
Baade Window ( $l = 1.13, b = -3.77$ )	13 Aug 1994	20, 200 ( $\times 2$ ), 1000 ( $\times 2$ )	undithered	18 03 10
	2 Sep 1995	40 ( $\times 2$ ), 200 ( $\times 4$ ), 400 ( $\times 3$ )	undithered	-29 51 45
	30 Aug 2000	40 ( $\times 8$ ), 400 ( $\times 8$ )	4-way dithered	
Sgr-I field ( $l = 1.25, b = -2.65$ )	21 Aug 1994	10, 100, 1000 ( $\times 3$ )	undithered	17 59 00.5
	8 Aug 2000	40 ( $\times 8$ ), 400 ( $\times 8$ )	4-way dithered	-29 12 14

Observations in 2000 obtained as part of this programme used filter F814W; of the archival 1994 and 1995 data sets, images obtained with the F814W were used for the proper motion determinations, and additionally F555W images were used for the color-magnitude diagrams.

Anderson & King (2000) and Ibata & Lewis (1998) describe ways in which astrometry can be performed in dense star fields using multiple dither observations. Essentially, these methods simultaneously derive a PSF (convolved with the pixel shape) that is consistent with the multiple dither observations of the same star field, and centroids for all stars in the field.

In the case of undersampled data, such as our first-epoch data, it is necessary to have independent knowledge of the shape of the PSF in order to be able to determine an accurate centroid. In dense star fields this information can be extracted provided the undersampling is not too severe: the stars will be positioned randomly with respect to the pixel grid of the detector, and so the ensemble of stars does in fact sample the PSF at a wide range of phases. Our method consists in a modification of the Anderson & King (2000) approach. For each exposure we start from an analytic PSF model, and determine best-fit centers and intensities for the 100 brightest unsaturated stars in the frame that are not affected by neighbours. These centers and intensities are then used to build an ensemble-averaged PSF from these stars. An analytic fit of somewhat higher order is then made to this new sampling of the PSF, with a robust outlier rejection. This new PSF is then used to define new centers and intensities, etc. This process iterates to convergence quite rapidly. In practice we use a gaussian PSF multiplied by polynomials as our model.

Armed with a PSF for each observation, we determine the proper motions as follows. First we combined all undithered data from the 1995 epochs, filter by filter, and identify  $20\text{-}\sigma$  detections in the combined image using the DAOFIND package. This master coordinate list for each CCD is then transformed using bright reference stars to align it with the positions in each individual exposure. For each F814W exposure a PSF fit is then performed near each transformed master list position, and the best-fit center and intensity recorded. The result is a set of up to 30 (21) position measurements for each star in the Baade Window (Sgr-I) fields, referred to the pixel positions of the different exposures, and spread over three (two) epochs.

These position measurements contain the proper motion information we seek, but also plate solution mappings from one exposure to another, and residual systematic centroiding errors. An iterative procedure, consisting of the following loop, separates the various effects: (i) find an average transformation that maps the star positions of each exposure onto those of a reference exposure, and apply this transformation to the positions; (ii) determine proper motions for each star based on these transformed positions, and determine position residuals for each position measurement from the best-fit proper motion; (iii) determine the average position residual as a function of pixel phase of each stellar image, and subtract this residual from each measurement; (iv) determine the average position residual as a function of phase with respect to the ‘34th-row’ effect (Anderson & King 1999) and subtract this. At each pass through the loop a new proper motion solution is made for each star, using a weighted linear least-squares fit with rejection of outliers. The weights are deduced from the estimated centroiding error of each image on the basis of the number of photons detected, including an estimated residual systematic error (see Figure 1).

Effects (iii) and (iv) are only detectable with dithered data, and so we have had to assume

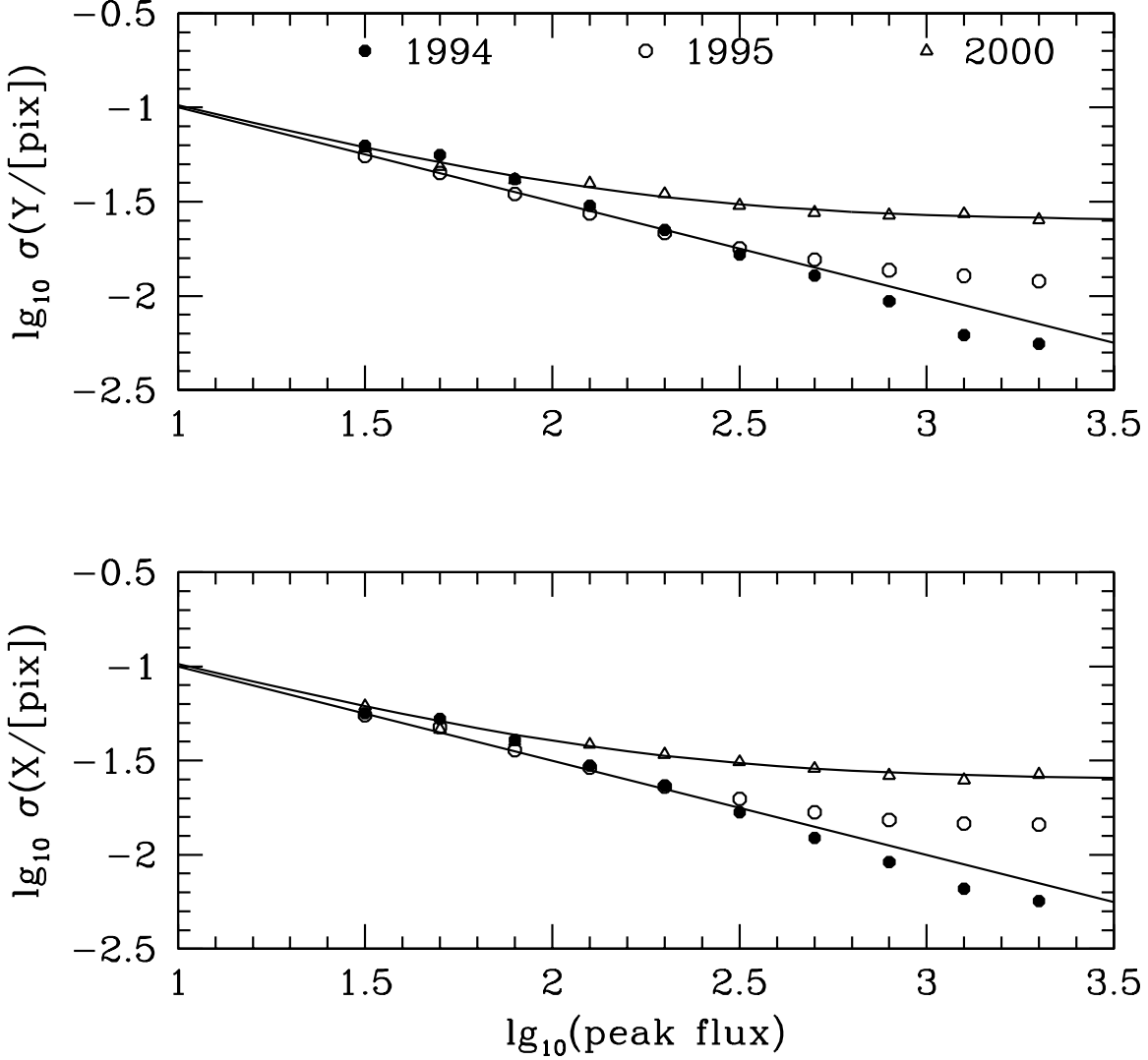


Fig. 1.— The rms residuals in  $x$  (top) and  $y$  (bottom) pixel position from the proper motion fits for the WF2 images of Baade’s Window. The plot illustrates that for the fainter stars the dominant source of error is photon noise, but that bright stars suffer from some residual systematic errors which are not removed by our procedure. This manifests itself as a higher residual error in the properly dithered, epoch 2000 data. The 1994 and 1995 data, which were not dithered, do not show this extra residual, indicating that any such systematics affecting those data have been absorbed into the proper motion fit. The solid lines represent a theoretical fit of the effect of photon statistics alone (lower line) and of an additional constant systematic error (upper curve). The upper curve has been used to generate error estimates on all positions and proper motions. A similar plot for PC data does not show such an additional systematic error.

that the systematic residuals with pixel phase and 34th-row phase (both on the order of 2–5% of a pixel) apply also to the earlier epochs. Any error we make in this assumption is not easily detectable in our data: any such positional error in the first epoch will simply be absorbed into the proper motion measurement. Two pieces of evidence give us confidence that our results are not seriously affected by such residual systematics:

1. The multiple dithers observed in our Y2K data provide a test of the procedure. With many dithered observations at the same epoch, residual errors show up as extra scatter about the best-fit position that cannot be absorbed into the proper-motion solution. Figure 1 shows that for the fainter stars our errors are safely dominated by photon statistics, and that systematic errors set in at the 0.03-pixel level on the undersampled WF detectors (corresponding to 20km/s over a 7-year baseline at the distance of the bulge).
2. Comparisons of the distributions of the proper motions between the PC and WF detectors shown below do not indicate that our WF proper motions contain larger errors than those derived from the PC.

Using this technique, we obtained proper motion measurements for some 20,000 stars in the Sgr-I field, and for 15,000 stars in Baade’s window. In addition, we used the 1994/1995 archival data for each field to derive magnitudes in the F814W and F555W filters, using the magnitude calibrations given in Holtzman et al. (1995).

Note that the proper motions derived are *relative*: we arbitrarily assign the mean proper motions of the complete sample of stars in each field to be zero in both components. Absolute (i.e., with respect to an inertial frame) proper motion measurements would require extragalactic sources such as qso’s to be identified in these fields. Perhaps future spectral or multi-color studies can provide this extragalactic reference frame.

### 3. Analysis

Proper motion distributions and color-magnitude diagrams are presented in Figures 2 and 3. The velocity dispersions per CCD are listed in table 2, and are consistent with each other—there is no indication of systematic differences between the velocity dispersions measured on the WF and PC CCD’s for the same fields, but there are field-to-field differences in the measured velocity dispersions. The proper motion distributions are skewed, with a longer tail towards positive  $\mu_l$ . We argue below that this is in large part due to foreground contamination.

At first inspection, the color-magnitude diagram shows a turnoff population with a blue extension and a red giant branch. A first cut at separating the kinematics of the various stellar populations can be attempted using those stars brighter than the old turnoff point, which we expect to show clear differences in kinematics (Figure 4). In fact, the blue main sequence stars have

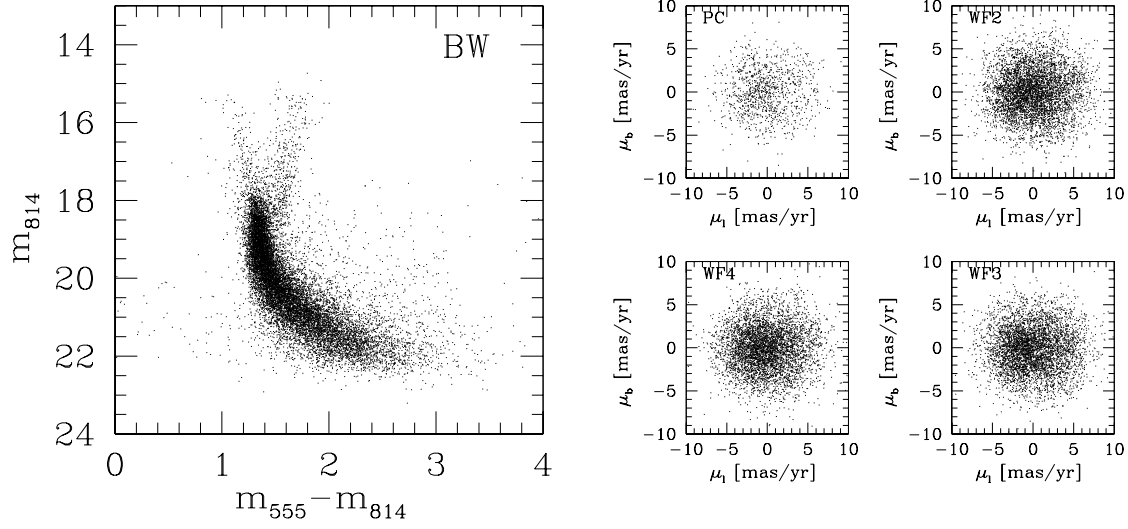


Fig. 2.— F814W/F555W color-magnitude diagram for the Baede Window field, and proper motion distributions for the individual CCD frames of the WF and PC.

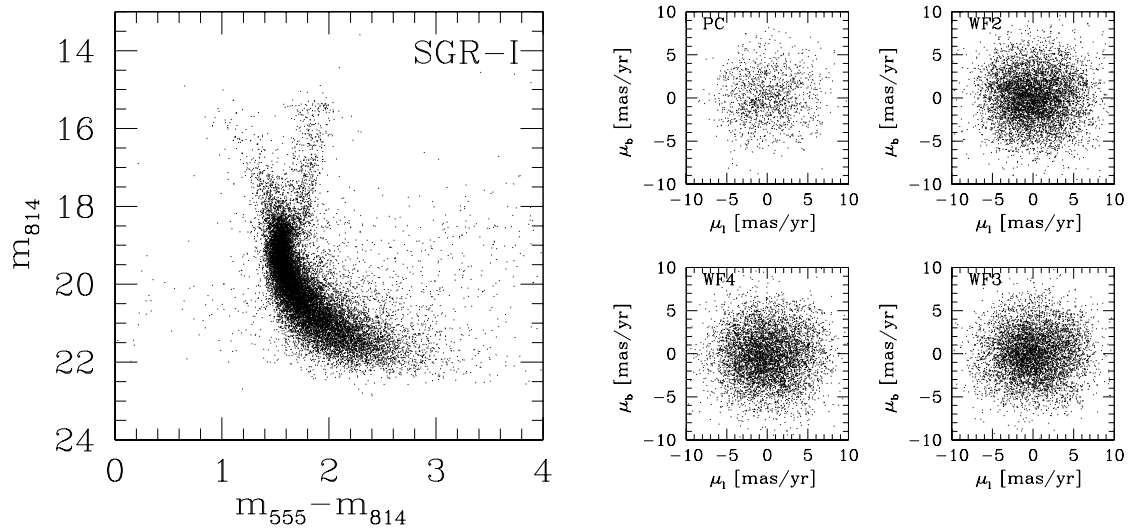


Fig. 3.— F814W/F555W color-magnitude diagram for the SGR-I field, and proper motion distributions for the individual CCD frames of the WF and PC.

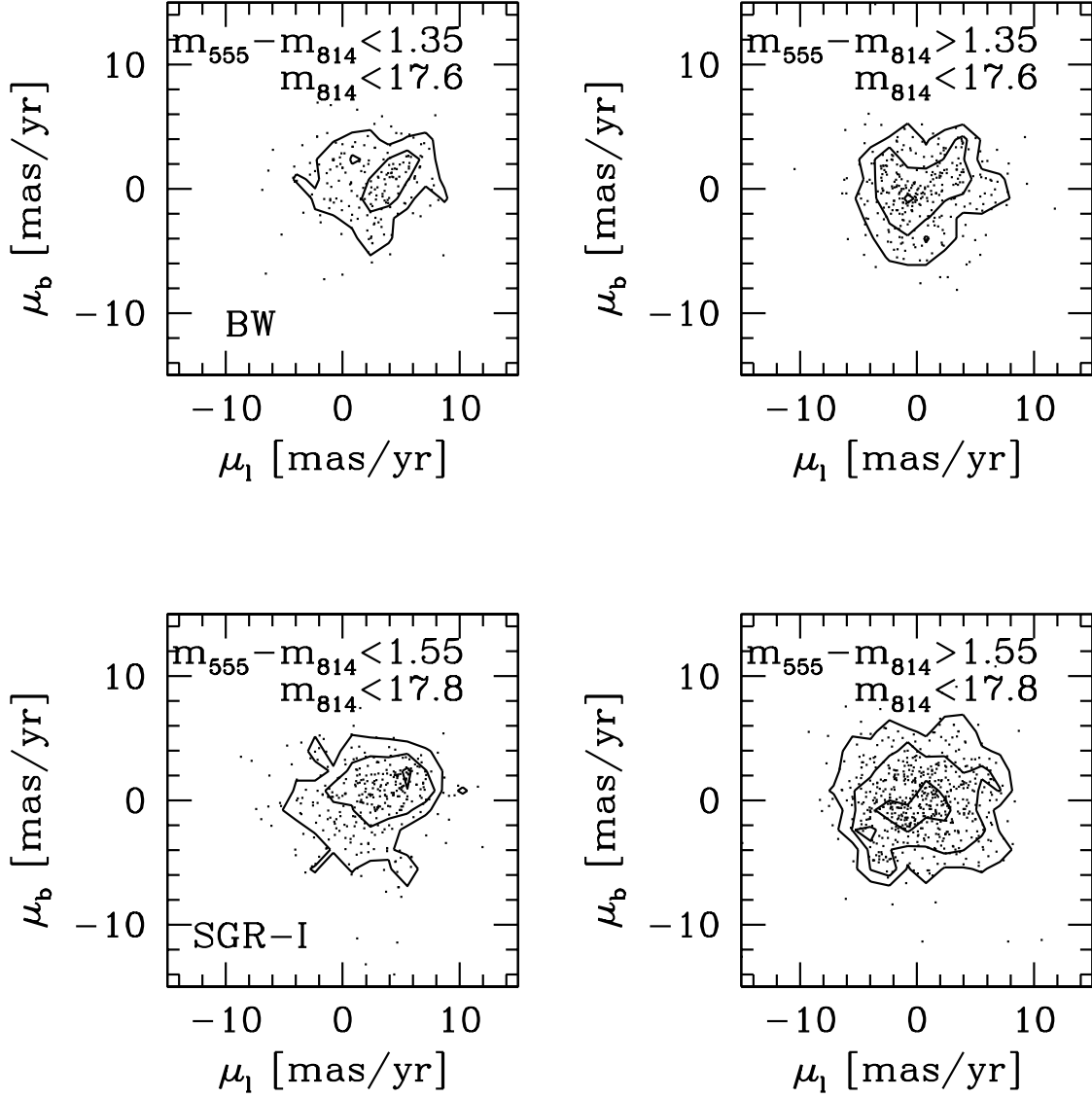


Fig. 4.— The proper motion distributions of blue (left) and red (right) giants in Baade’s Window (top) and the Sgr-I field (bottom). In both fields the blue giants show a marked proper motion offset in the positive longitude direction, as expected for a foreground population rotating in front of the bulge. The red giants do not show this effect, suggesting they represent the dominant population in these bulge windows.



a mean positive longitudinal proper motion of some 5mas/yr with respect to the red giants. This is most simply understood as a foreground, thin disk population which rotates in front of the bulge stars.

The bright blue main sequence stars are the part of the younger disk population that stand out in the color-magnitude diagram (CMD), but of course disk stars are found among fainter stars as well. This is best illustrated in Figs. 5 and 6, which are binned color-magnitude diagrams, with each bin color-coded by various kinematic quantities. These figures clearly show the extent of disk contamination across the CMD, as well as a number of other kinematic features:

1. The disk kinematics of the bright blue main sequence stars (large positive  $\mu_l$ ) are shared by redder, fainter stars located above the bulge main sequence. This is naturally explained as the main sequence of disk stars in front of the bulge. As expected, the effect is more pronounced in the Sgr-I field, which lies closer to the galactic plane.
2. There is a gradient in the mean  $\mu_l$  of faint main sequence stars with magnitude: at a given color, the faintest main sequence stars drift towards negative  $l$ . This suggests that we are measuring stars clear through the bulge rotation field, even to the far side of the bulge, where stars are rotating behind the galactic minor axis.
3. The proper motion dispersions of the main sequence stars decrease with magnitude: at a given color the faintest main sequence stars have smaller dispersion in proper motion. We interpret this as a distance effect: the faintest stars are further away and hence a given velocity translates into a smaller proper motion.
4. There is a distinct suggestion in these diagrams of a kinematically homogeneous bulge population which follows a single isochrone, characteristic of an old stellar population.

In order to investigate the kinematics further, we make cuts of main sequence stars for which

Table 2: Proper motion dispersions (mas yr<sup>-1</sup>) by field

Field	Baade Window			SGR-I Field		
	$N$	$\sigma_l$	$\sigma_b$	$N$	$\sigma_l$	$\sigma_b$
PC	1076	2.91±0.06	2.51±0.05	1388	3.10±0.06	2.73±0.05
WF2	5036	2.98±0.03	2.59±0.03	6583	3.25±0.03	2.78±0.03
WF3	4848	3.00±0.03	2.53±0.03	6156	3.23±0.03	2.71±0.03
WF4	4902	2.97±0.03	2.53±0.03	6107	3.27±0.03	2.84±0.03
All	15862	2.98±0.017	2.54±0.014	20234	3.24±0.016	2.77±0.014

Mean proper motions have not been measured. None of the samples shows significant evidence for a misalignment of the principal kinematic axes with galactic coordinates, i.e., we detect no covariance between  $\mu_l$  and  $\mu_b$ .

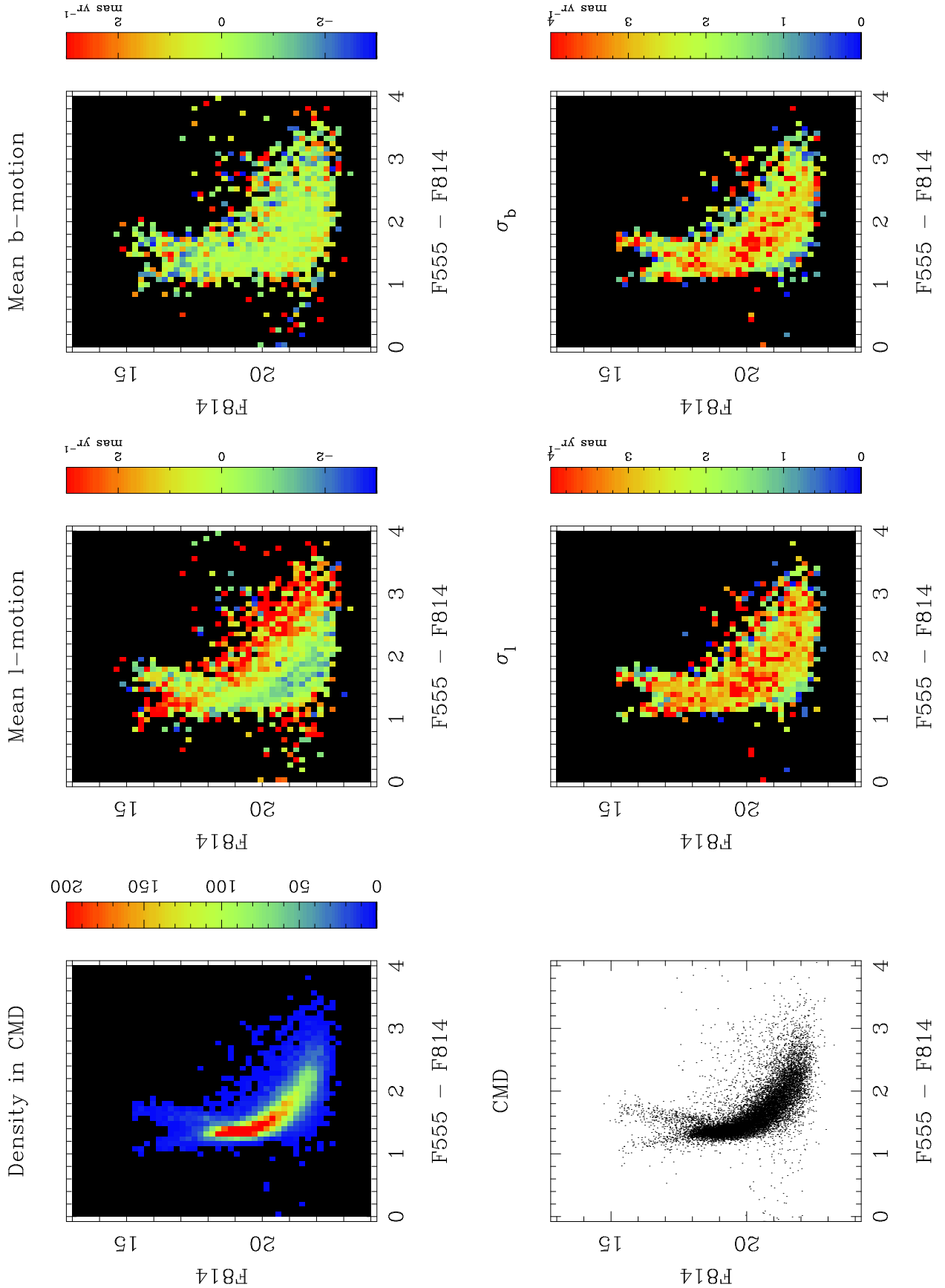


Fig. 5.— Binned color-magnitude diagrams of Baade’s Window. The sample is plotted in each panel color-coded in different ways. Top row (left to right): number of stars in each bin; mean

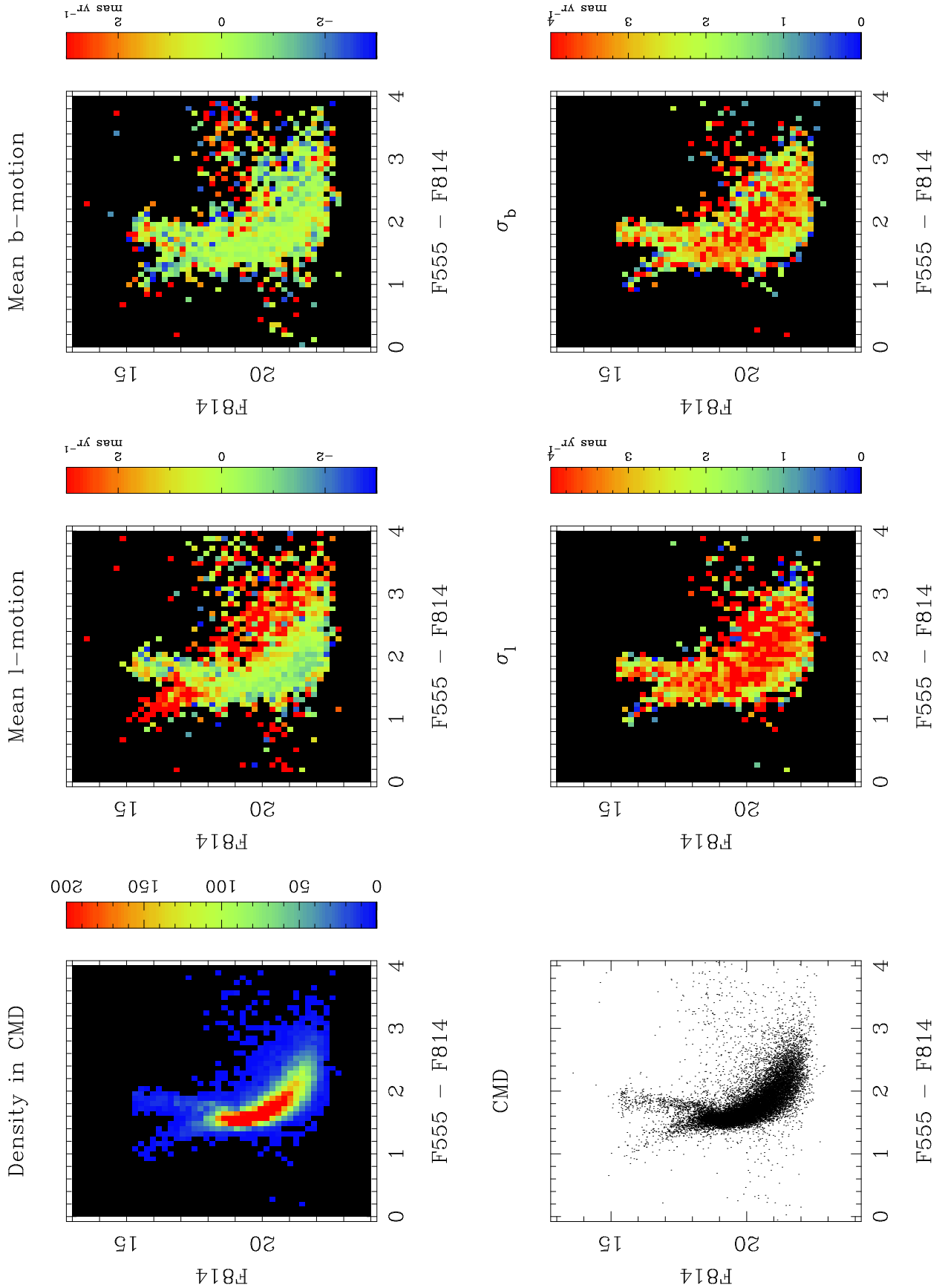


Fig. 9.— Binned color-magnitude diagrams of the Sgr I field. The sample is plotted in each panel color-coded in different ways. Top row (left to right): number of stars in each bin; mean

a crude distance modulus can be calculated. We find that the quantity

$$M^* = m_{F814W} - 2(m_{F814W} - m_{F555W})$$

removes the slope of the main sequence in the CMD, so that it may be used as a simple relative distance indicator. As a function of this distance modulus we plot the proper motions in Figs. 7 and 8. In both Baade’s Window and Sgr I, the same picture emerges. We see a smooth gradient of rotation down the line of sight. This is either due to contamination of a non-rotating bulge by disk stars, or represents a true rotation of the bulge. The notable similarity of the slope of both ‘rotation curves’ in both fields (even though the Sgr-I field is expected to be more disk-dominated) argues for an intrinsic bulge rotation.

Radial velocity surveys find rotation in the bulge population; perhaps the best example is that of Izumiura et al. (1995), which shows the rotation curve based on a survey of SiO masers. The practical difficulty with measuring the rotation curve of the *pure bulge* population is that as one moves off-axis, the density of the bulge drops rapidly and sample contamination (from the halo and disk) becomes a major problem. Our study gives one of the cleanest demonstrations of rotation in a bulge star dominated sample.

Some undulations in the vertical mean proper motion are also seen. There is the hint of a rise in the vertical proper motion for those stars which might correspond to the “middle” of the bulge. At this point it is not clear whether these trends in the vertical mean proper motion are real, or a manifestation of an unknown systematic residual error.

It is notable that the proper motion dispersions decrease for the faintest  $M^*$ . This is as expected if these stars are indeed at larger distances: these stars would lie a factor two further away than stars with  $M^*$  ca. 1.5 magnitudes brighter.

Detailed modelling of these results is complicated by the uncertain scatter in these crude photometric parallaxes. However, we can estimate values for the velocity dispersions of bulge stars in each field by considering the  $M^*$  bin with zero mean  $\mu_l$ . These stars should lie as close to the Galactic minor axis as these lines of sight reach. The numbers are given in Table 3. We see evidence for a subtle anisotropy in the bulge, but this could be an effect of the velocity gradient through the  $M^*$  bin.

The tangential dispersions in Table 3 are similar to those for the full sample (Table 2). This coincidence is caused by two effects which act in opposite directions. The full sample contains many distant stars, whose proper motions are small and hence reduce the dispersion; on the other

Table 3: Proper motion dispersions in km/sec (for  $R_0 = 8\text{kpc}$ )

	$\sigma(\mu_l)$	$\sigma(\mu_b)$	$\sigma_l$	$\sigma_b$
Baade Window	2.94	2.63	111	100
Sgr-I Field	3.24	2.85	123	108

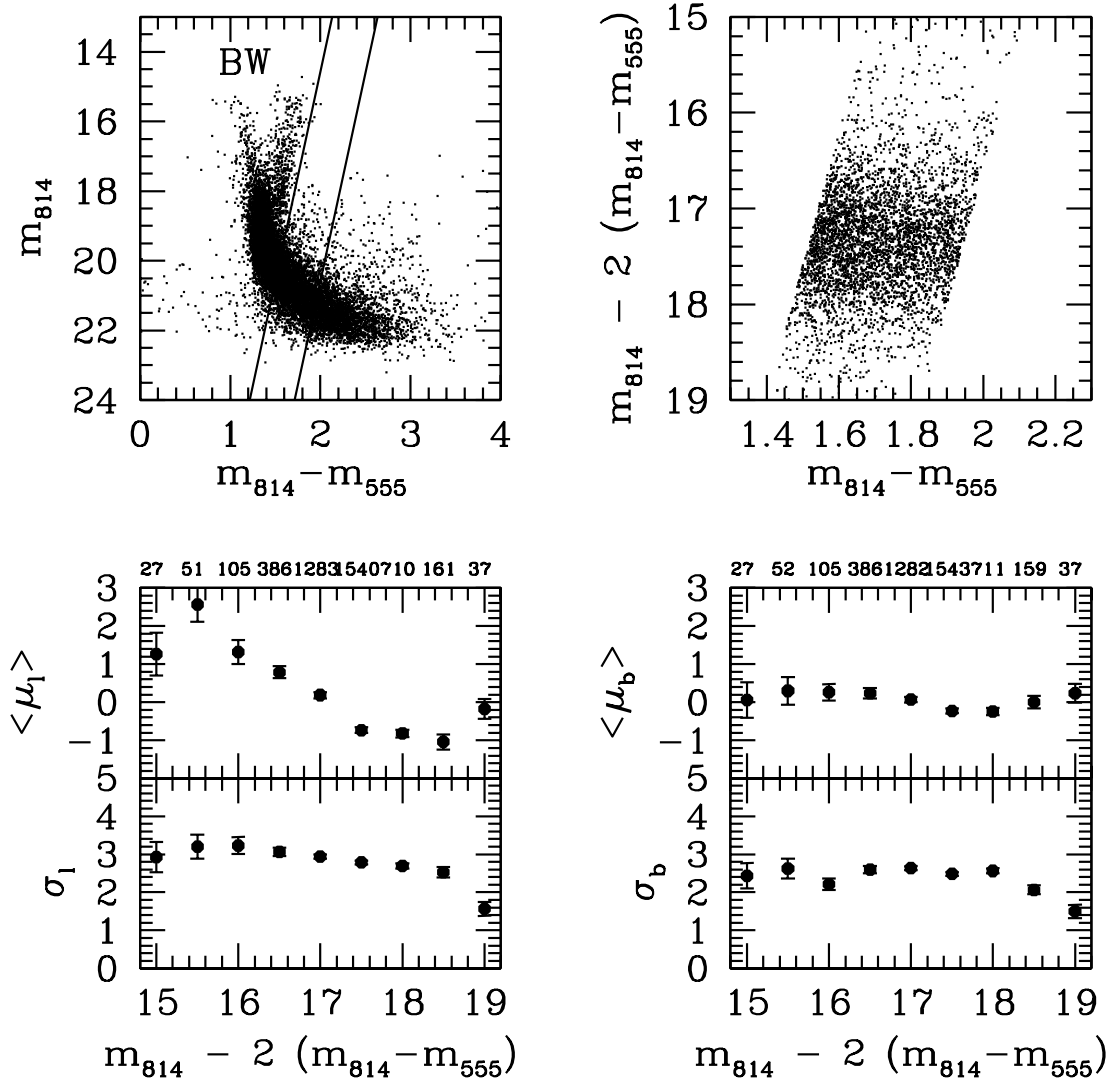


Fig. 7.— The proper motion statistics in Baade’s window versus the distance estimator  $M^*$ . Top left: the CMD with the selection region of stars. Top right: demonstration of the independence of  $M^*$  with color. Bottom left: Mean and dispersion in  $\mu_l$  in ‘distance’ bins. Bottom right: Mean and dispersion in  $\mu_b$  in ‘distance’ bins.

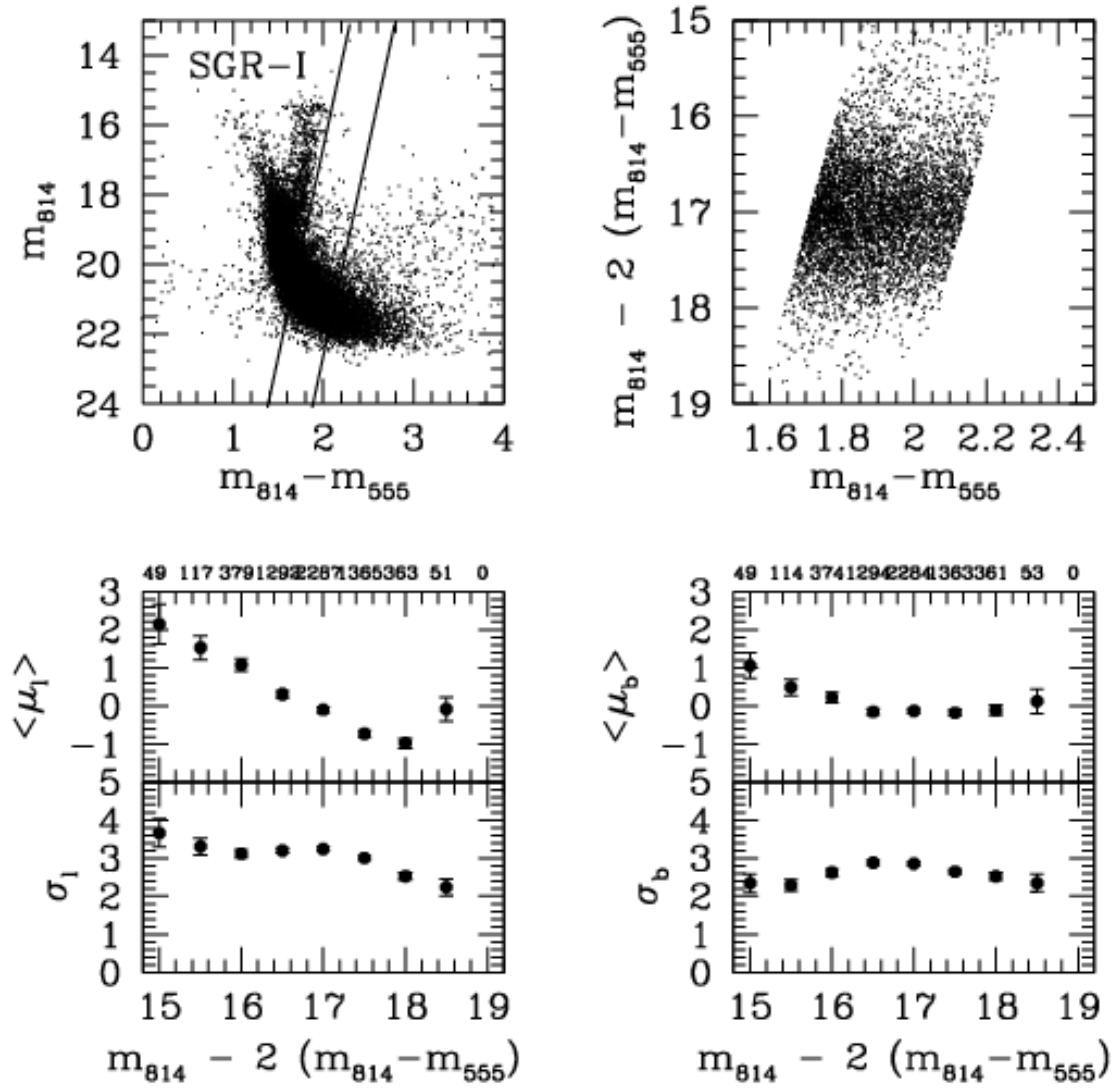


Fig. 8.— As in Figure 7, but for the Sgr-I field.

hand the line-of-sight gradient in tangential velocity tends to increase the width of the distribution. Only the first effect operates in the vertical direction, so  $\sigma(\mu_b)$  values are larger in Table 3 than they are in the full sample.

#### 4. The stellar population of the bulge

With our picture of the kinematics in the bulge region, we now study the stellar populations. We isolate a “pure bulge” sample by keeping only stars with negative  $\mu_l$  and moderate  $|\mu_b|$ . Given the rotation gradient of the bulge, this kinematic cut may also preferentially remove near-side bulge stars from the sample, so it may be slightly biased in distance. Far-side disk contamination should be very small as the line of sight rises away from the galactic plane behind the bulge.

The color-magnitude diagrams that these cuts produce in Baade’s Window and the Sgr I field are shown in Figure 9. The  $\mu_l, \mu_b$  cuts cleanly remove the bright blue portion of the main sequence and foreground M dwarfs, by kinematic selection only. The color-magnitude diagram that remains strongly resembles that of the old bulge globular cluster NGC 6553 (cf. Zoccali et al. 2001). A handful of stars brighter than the old turnoff remain (field blue stragglers or outliers?) but the dominant blue extension is clearly demonstrated to be a foreground population. The present color-magnitude diagram suggests that blue stragglers are not common in the field population (for example, not nearly as frequent as found in the cluster NGC 6553 by Zoccali et al. 2001). However, it does not put interesting limits on their numbers. To do so would require radial velocities and perhaps line strength measurements. When additional analysis is finished, we will be able to derive the age of the bulge field relative to NGC 6553 and 6528; a cursory examination of Figure 9 shows the characteristic turnoff point of a clearly old stellar population.

The impression that two very different populations are being identified via the proper motions is amplified when one considers the luminosity functions for the bulge and disk populations. Recall that (especially at the bright end) incompleteness and photometric errors are identical, being only magnitude dependent. Figure 10 shows our plot for the Baade’s Window disk and bulge samples, and the disk’s extension (relative to the sharp rise of the main sequence turnoff) is evident. These plots give further strength to the visual impression from Figure 9.

We emphasize that our population separation is based on kinematics, not on any photometric or spectroscopic classification. While disk and bulge exist cospatially, they separate well kinematically, and this is therefore at least a complementary, and we would argue a more robust, technique for isolating a ‘pure bulge’ population.

## 5. Conclusions

With HST photometry and proper motions determined with high enough precision, it is possible to separate the disk and bulge populations by their kinematics alone. The long standing question regarding the nature of the blue main sequence extension in the bulge field population is settled: the great majority of those stars evidently belong to the foreground disk. When these stars are excluded, the old turnoff population in the bulge remains, and no measureable population of blue stragglers or intermediate age stars is present. This was first demonstrated for the Baade’s Window field by Ortolani et al. (1995). Feltzing & Gilmore (2000) came to the same conclusion based on counts of stars brighter and fainter than the turnoff point in their WFPC2 data. However, a proper accounting for the foreground disk has been a persistent issue, and our application of the kinematic data strengthens greatly the conclusion that the bulge is dominated by old stars.

We take our study a step further, and find direct evidence for the rotation of the bulge population. The observed proper motion anisotropy of bulge stars is largely caused by the line-of-sight gradient of the rotation of the bulge; when this is removed a nearly isotropic velocity distribution of the bulge stars results. The velocity dispersion declines from Sgr I to Baade’s Window.

When appropriate samples in Baade’s Window are compared, our proper motion dispersions agree with those found by Spaenhauer, Jones, & Whitford (1992) and by Feltzing & Johnson (2001). Our results compare well with predictions of the Zhao (1996) and Zhao, Rich, & Spergel (1996) bulge model, but since our proper motion samples are more than an order of magnitude larger than existing radial-velocity and proper-motion samples of bulge stars, and extend well below the turnoff, the time is ripe for more involved modelling. Extension of this work to further bulge fields (e.g. Zoccali et al. 2001), and combination of these results with spectroscopy (for radial velocities, metallicity, and improved distance estimates) should open the way for a new chapter in our study of the Galactic bulge.

Support to RMR for proposal GO-8250 was provided by NASA through a grant from the Space Telescope Science Institute, which is operated by the Association of Universities for Research in Astronomy, Inc., under NASA contract NAS 5-26555.

### A. Accuracy of PSF-fitting photometry and positions

Here we calculate the accuracy of object centroids derived by means of PSF fitting.

Let  $f_i$  be the data: intensities on the pixels  $i$  at positions  $x_i, y_i$  on the image plane. We try to model these data as  $AP(x_i - \mu_x, y_i - \mu_y)\Delta^2$ , where  $\Delta$  is the pixel width, and  $P$  is the PSF normalized to total intensity 1.  $A$  is the intensity of the star, and  $(\mu_x, \mu_y)$  are the position of the



star, to be fitted for. Write

$$\chi^2 = \sum_i (f_i - AP(x_i - \mu_x, y_i - \mu_y)\Delta^2)^2 / \sigma_i^2$$

where  $\sigma_i$  is the error on the measured intensity in pixel  $i$ . Then the minimum of  $\chi^2$  gives the best-fit PSF, and the second partial derivatives of  $\chi^2$  with respect to any two parameters give twice the inverse covariance matrix. In what follows we ignore covariances between the different variables  $A$ ,  $\mu_x$  and  $\mu_y$ , as is appropriate for bisymmetric PSF's.

At the best-fit value (we may assume without loss of generality that  $\mu_x = \mu_y = 0$ ) we obtain the inverse variance on the star's intensity  $A$  as

$$\text{Var}(A)^{-1} = 0.5\partial^2\chi^2/\partial A^2 = \sum_i P(x_i, y_i)^2\Delta^4/\sigma_i^2$$

which reduces to

$$= \left( \int P^2 dx dy \right) \Delta^2 / \sigma^2$$

if the PSF is fully sampled and  $\sigma_i$  constant (i.e., background- or read noise-limited data).

The inverse variance of the best-fit position is similarly (removing terms which go to zero at the best fit)

$$\text{Var}(\mu_x)^{-1} = 0.5\partial^2\chi^2/\partial\mu_x^2 = \sum_i A^2(\partial P/\partial x)^2\Delta^4/\sigma^2 = \left( \int (\partial P/\partial x)^2 dx dy \right) A^2\Delta^2/\sigma^2$$

(and similarly for  $\mu_y$ ). These two relations can be combined to give

$$\delta\mu_x = \frac{\delta A}{A} \times \sqrt{\frac{\int P^2 dx dy}{\int (\partial P/\partial x)^2 dx dy}}$$

where  $\delta A = \text{Var}(A)^{-1/2}$  is the 1- $\sigma$  error on  $A$ , etc.

The centroid error therefore depends on the significance  $A/\delta A$  of the detection of the star, and on a geometric factor governed only by the shape of the PSF.

For a gaussian PSF, dispersion  $s$ , we find

$$\text{Var}(A)^{-1} = \Delta^2/(4\pi s^2\sigma^2)$$

hence

$$\delta A = \sqrt{4\pi} s \sigma / \Delta$$

and

$$\text{Var}(\mu_x)^{-1} = A^2\Delta^2/(8\pi s^4\sigma^2)$$

hence

$$\delta\mu_x = \sqrt{8\pi}s^2\sigma/(\Delta A) = \sqrt{2}s\frac{\delta A}{A}$$

For a Moffat function PSF of the form

$$P = \frac{\beta - 1}{\pi a^2} \left(1 + \frac{r^2}{a^2}\right)^{-\beta}$$

we get

$$\delta\mu_x = a\frac{\delta A}{A} \sqrt{\frac{2\beta + 1}{\beta(2\beta - 1)}}$$

If we write  $a$  as  $\frac{1}{2}\text{FWHM}/\sqrt{2^{1/\beta} - 1}$ , we find that for  $\beta > 1.5$ , which covers PSF's with tails as shallow as  $r^{-3}$

$$\delta\mu_x = \frac{\delta A}{A} \times 0.67 \times \text{FWHM} \pm 10\%.$$

(The gaussian is the limit  $\beta \rightarrow \infty$ ; in this case the coefficient is 0.6.)

## REFERENCES

- Alcock, C. et al. 2000, ApJ, 541, 734
- Anderson, J. & King, I. R. 2000, PASP, 112, 1360
- Anderson, J. & King, I. R. 1999, PASP, 111, 1095
- Arp, H. 1965, ApJ, 141, 43
- Dwek, E. et al. 1995, ApJ, 445, 716
- Feltzing, S., & Gilmore, G. 2000, *a*, 355, 949
- Feltzing, S. & Johnson, R. 2002, A&A, in press.
- Holtzman, J. A., Burrows, C. J., Casertano, S., Hester, J. J., Trauger, J. T., Watson, A. M., & Worthey, G. 1995, PASP, 107, 1065
- Holtzman, J. A., Watson, A. M., Baum, W. A., Grillmair, C. J., Groth, E. J., Light, R. M., Lynds, R., & O'Neil, E. J. 1998, AJ, 115, 1946
- Ibata, R. A. & Lewis, G. F. 1998, AJ, 116, 2569
- Izumiura, H., Deguchi, S., Hashimoto, O., Nakada, Y., Onaka, T., Ono, T., Ukita, N., & Yamamura, I. 1995, ApJ, 453, 837
- McWilliam, A. & Rich, R. M. 1994, ApJS, 91, 749

Ortolani, S., Renzini, A., Gilmozzi, R., Marconi, G., Barbuy, B., Bica, E., & Rich, R. M. 1995, *Nature*, 377, 701

Spaenhauer, A., Jones, B. F., & Whitford, A. E. 1992, *AJ*, 103, 297

Zhao, H. S. 1996, *MNRAS*, 283, 149

Zhao, H., Rich, R. M., & Spergel, D. N. 1996, *MNRAS*, 282, 175

Zoccali, M., Renzini, A., Ortolani, S., Bica, E., & Barbuy, B. 2001, *AJ*, 121, 2638

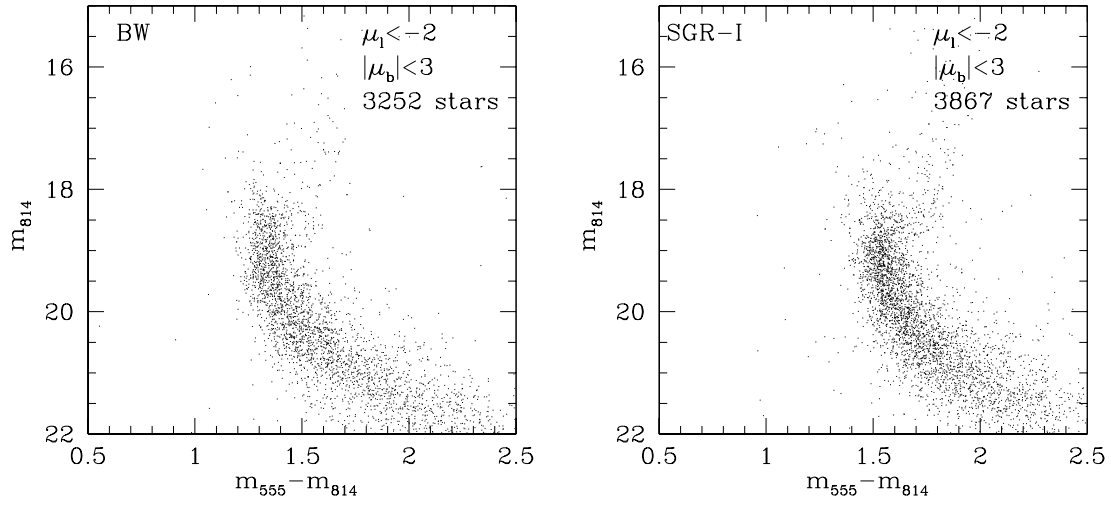


Fig. 9.— The color-magnitude diagrams for kinematically-selected bulge stars the two fields. The stars plotted are subsamples selected kinematically against disk stars. The cut in  $\mu_l$  removes foreground stars with kinematics such as those of the blue giants, while the  $\mu_b$  upper limit cuts nearby M dwarfs seen particularly in the Sgr-I field.

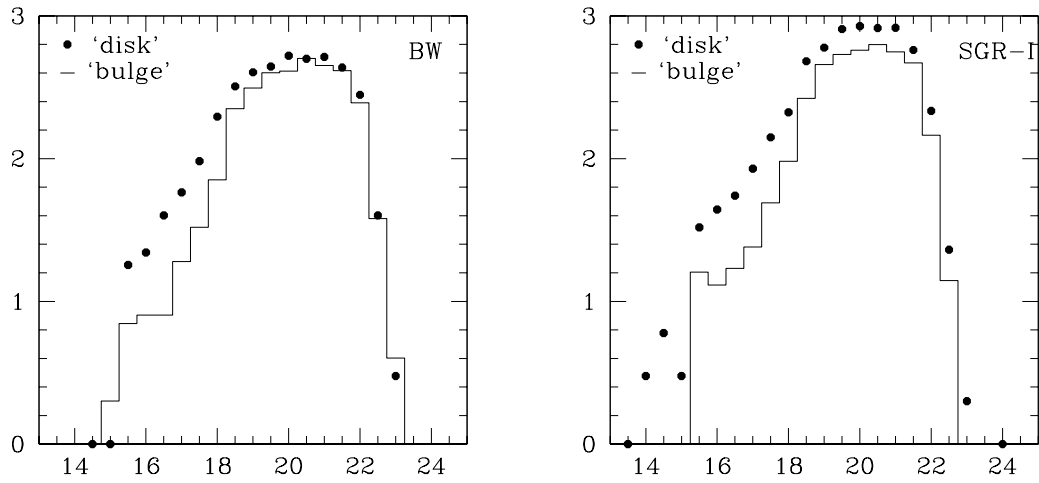


Fig. 10.— Differential luminosity functions for stars selected according to the kinematic cuts used in Figure 9. The shallower slope of the luminosity function at the bright end is presumably due to an excess of young and intermediate age stars in the disk, relative to the bulge (which rises steeply at the old turnoff point). We emphasize that the differences are measured from stars in the same images and are present at the same magnitude; therefore they cannot be due to image crowding or incompleteness errors. Notice the similarities between the two fields, especially the steepness of the turnoff rise.